Bioactive Materials 6 (2021) 3383–3395

Contents lists available at ScienceDirect

Bioactive Materials

journal homepage: www.sciencedirect.com/journal/bioactive-materials

In vitro characterization of novel nanostructured collagen-hydroxyapatite composite scaffolds doped with magnesium with improved biodegradation rate for hard tissue regeneration

Iulian V. Antoniac [a,b], Aurora Antoniac [a,*], Eugeniu Vasile [a,**], Camelia Tecu [a], Marco Fosca [c], Viktoriya G. Yankova [d], Julietta V. Rau [c,d,***]

[a] University Politehnica of Bucharest, 313 Splaiul Independentei Street, District 6, 060042, Bucharest, Romania
[b] Academy of Romanian Scientists, 54 Splaiul Independentei Street, District 5, 050094, Bucharest, Romania
[c] Istituto di Struttura della Materia, Consiglio Nazionale delle Ricerche (ISM-CNR), Via del Fosso del Cavaliere, 100, 00133, Rome, Italy
[d] Sechenov First Moscow State Medical University, Institute of Pharmacy, Department of Analytical, Physical and Colloid Chemistry, Trubetskaya 8, Build. 2, Moscow, 119991, Russia

ARTICLE INFO

Keywords:
Composite
Collagen
Hydroxyapatite
Magnesium
Scaffold
Hard tissue regeneration
Scaffold degradation

ABSTRACT

New materials are required for bone healing in regenerative medicine able to temporarily substitute damaged bone and to be subsequently resorbed and replaced by endogenous tissues. Taking inspiration from basic composition of the mammalian bones, composed of collagen, apatite and a number of substitution ions, among them magnesium (Mg^{2+}), in this work, novel composite scaffolds composed of collagen(10%)-hydroxyapatite (HAp)(90%) and collagen(10%)-HAp(80%)-Mg(10%) were developed. The lyophilization was used for composites preparation. An insight into the nanostructural nature of the developed scaffolds was performed by Scanning Electron Microscopy coupled with Energy Dispersive X-Ray and Transmission Electron Microscopy coupled with Energy Dispersive X-Ray. The HAp nanocrystallite clusters and Mg nanoparticles were homogeneously distributed within the scaffolds and adherent to the collagen fibrils. The samples were tested for degradation in Simulated Body Fluid (SBF) solution by soaking for up to 28 days. The release of Mg from collagen (10%)-HAp(80%)-Mg(10%) composite during the period of up to 21 days was attested, this composite being characterized by a decreased degradation rate with respect to the composite without Mg. The developed composite materials are promising for applications as bone substitute materials favouring bone healing and regeneration.

1. Introduction

In the frames of regenerative medicine topics and, more specifically, in bone healing branch, over the last decades, the aim of research was to develop an ideal material, able to temporarily substitute damaged bones and to be subsequently resorbed and replaced by endogenous tissues. This trend is confirmed by the numerous reviews highlighting recent advances in bone tissue engineering and progress in clinical translation of scaffold and ceramic devices for bone regeneration [1,2]. Such an ideal material has to meet several requirements, among them, adequate mechanical properties, biocompatibility and ability to promote osteogenesis process [3,4]. Natural mammalian bone matrix is mainly composed of two constituents, such as collagen and calcium-deficient hydroxyapatite (CdHAp) [5]. In addition to these main constituents, several substitution ions, such as carbonate (CO_3^{2-}) [6], strontium (Sr^{2+}) [7,8] and magnesium (Mg^{2+}) [9,10] are present in CdHAp, each one of them playing a specific functional role [11–13]. Mimicking the basic composition of the mammalian bones it comes natural that researchers try to develop a suitable material starting from the collagen-hydroxyapatite (collagen-HAp) composite [14]. According to a

Peer review under responsibility of KeAi Communications Co., Ltd.
* Corresponding author.
** Corresponding author.
*** Corresponding author. Istituto di Struttura della Materia, Consiglio Nazionale delle Ricerche (ISM-CNR), Via del Fosso del Cavaliere, 100, 00133, Rome, Italy.
E-mail addresses: aurora.antoniac@upb.ro (A. Antoniac), eugeniu.vasile@upb.ro (E. Vasile), giulietta.rau@ism.cnr.it (J.V. Rau).

https://doi.org/10.1016/j.bioactmat.2021.02.030
Received 17 September 2020; Received in revised form 15 February 2021; Accepted 23 February 2021

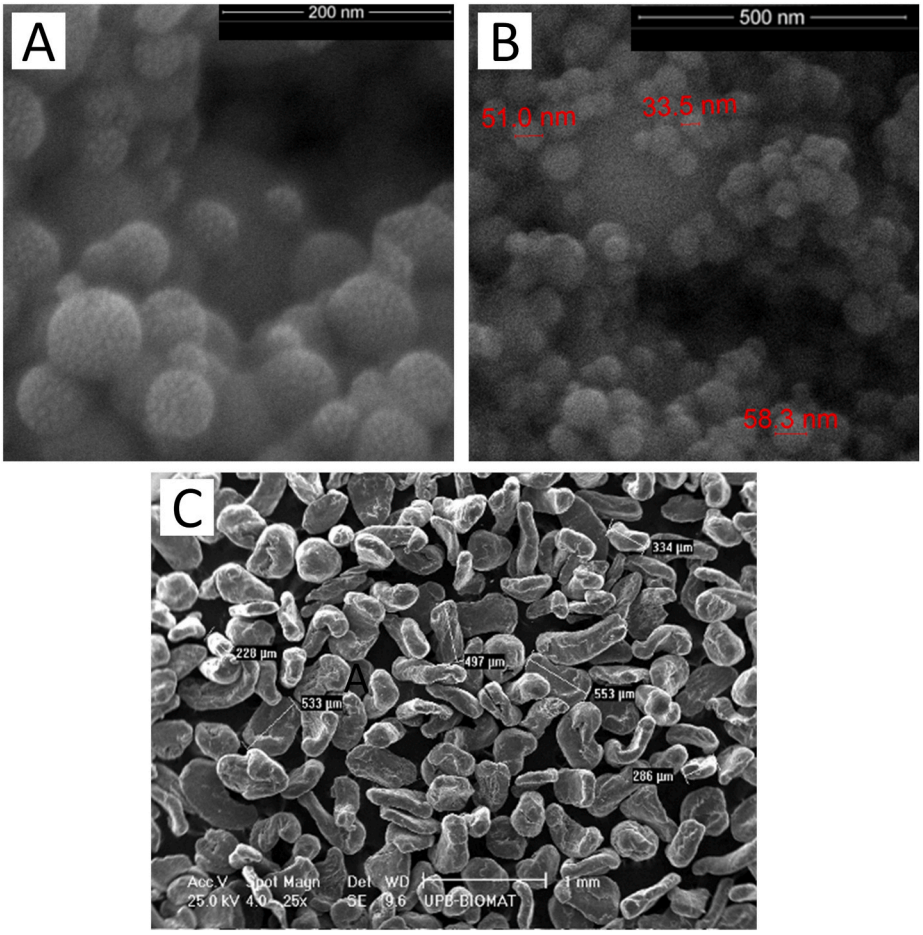

Fig. 1. SEM images of initial HAp(A,B) and Mg(C) powders.

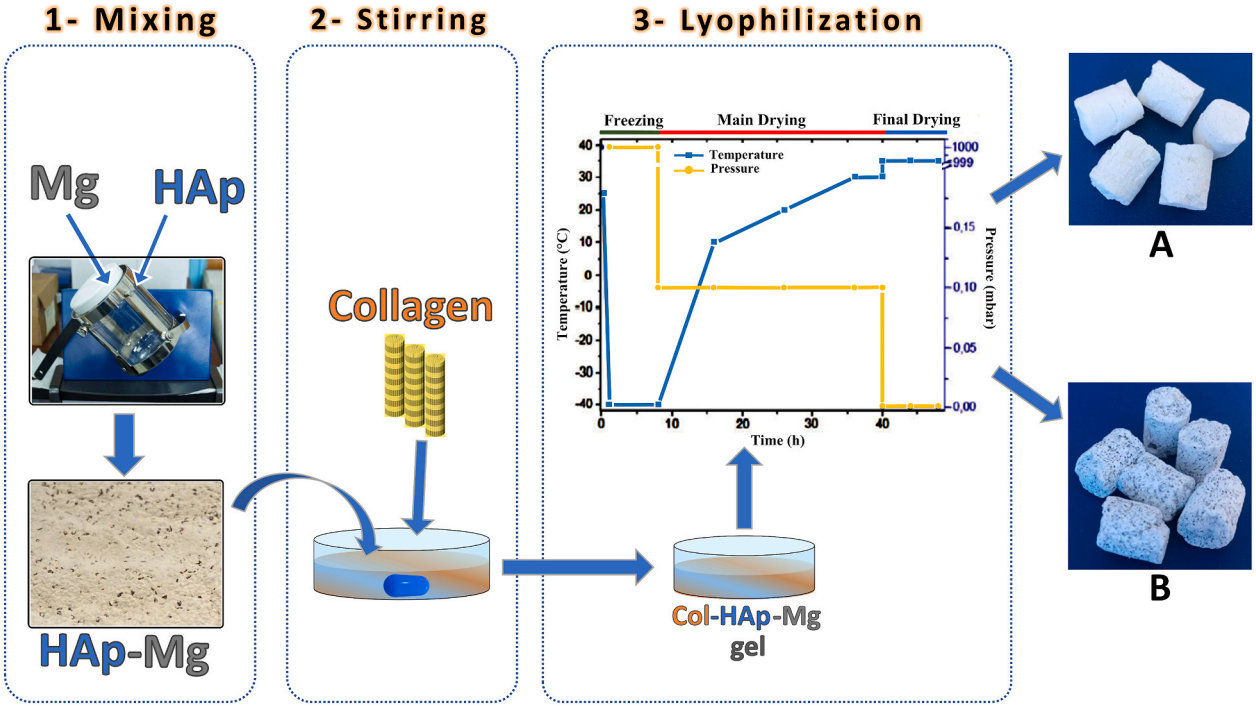

Fig. 2. Flowchart with the processing steps. On the right side, A (collagen-HAp) and B (collagen-HAp-Mg) final samples.

Table 1
Biodegradation of P1 and P2 in SBF.

Sample Code	Immersion time (days)	pH[a]
P1_1	1	7.1 ± 0.3
P1_7	7	7.1 ± 0.2
P1_14	14	7.1 ± 0.2
P1_21	21	7.1 ± 0.1
P1_28	28	7.1 ± 0.2
P2_1	1	8.2 ± 0.2
P2_7	7	9.1 ± 0.1
P2_14	14	9.4 ± 0.3
P2_21	21	9.2 ± 0.1
P2_28	28	9.5 ± 0.1

[a] The pH values are the averages for three determinations ± standard deviations.

recent trend of scientific community, a third component is included into collagen-HAp composite, in order to improve its properties and to develop an optimal bone-substitute material to be used as bone filler, bone scaffold or both of them.

Socrates et al. [15] proposed a fibrillar shaped matrix of collagen-HAp loaded with silver (Ag) nanoparticles. The composite material was obtained by first including Ag nanoparticles in a collagen matrix, and subsequently soaking it in Simulated Body Fluid (SBF), in order to promote mineralization with the formation of biomimetic HAp on the matrix surface. The Ag containing compound exhibited enhanced mechanical properties and good antibacterial ability along with biocompatibility towards MG-63 and red blood cells. Predoi et al. [16] reported a study where a composite of Ag-substituted HAp (0.1% Ag) was added to a collagen gel. Also in this case, the Ag-containing bio-composite showed antibacterial characteristics.

Aryal et al. [17] reported HAp growth on self-assembled collagen gold (Au) nanoparticles, providing crystallographic investigation of the Au/HAp/collagen compound. It was found that the HAp crystals grew

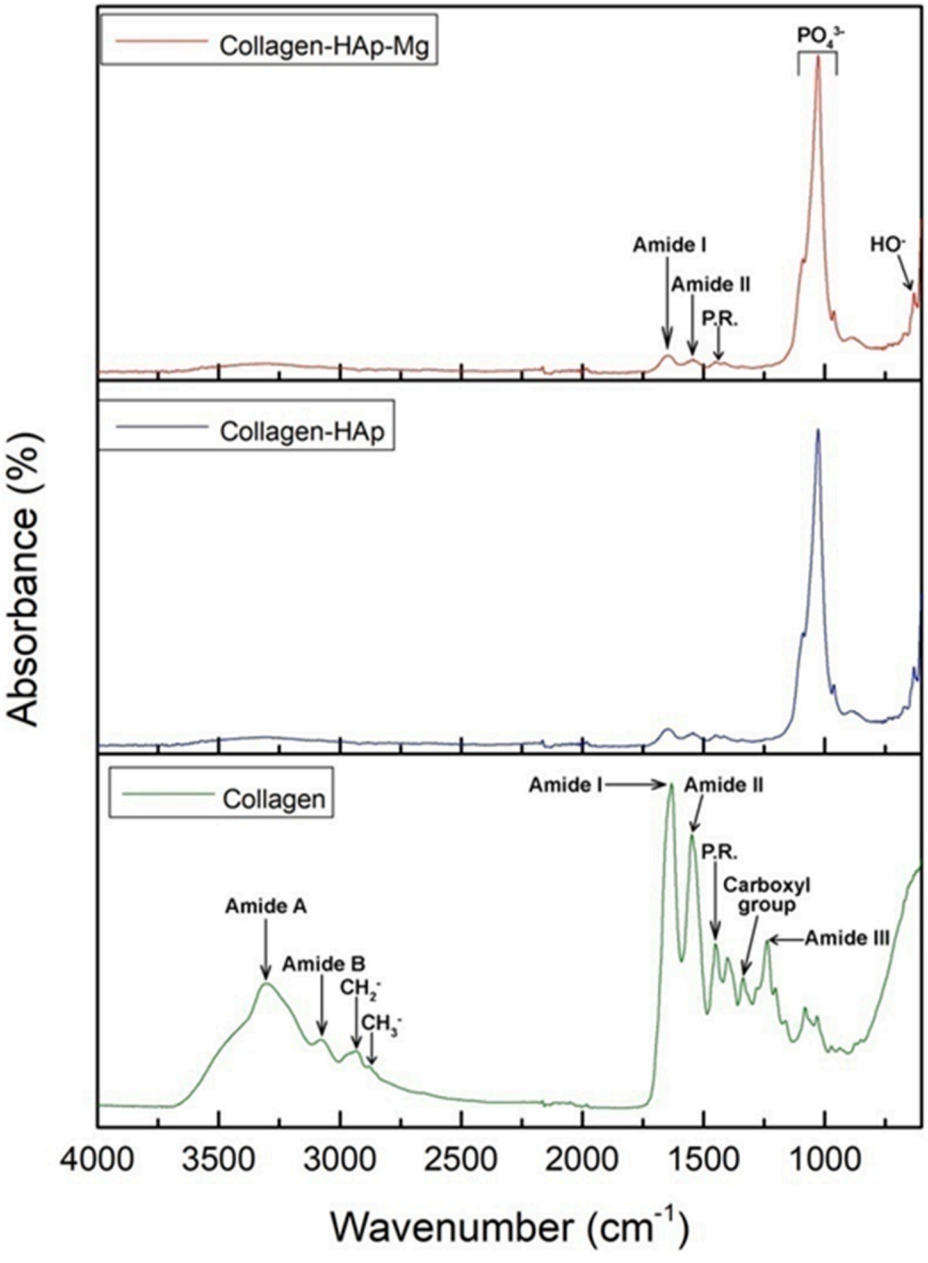

Fig. 3. FTIR spectra of the collagen alone and of the composite collagen-HAp and collagen-HAp-Mg biomaterials. P.R. stands for the pyrrolidine rings.

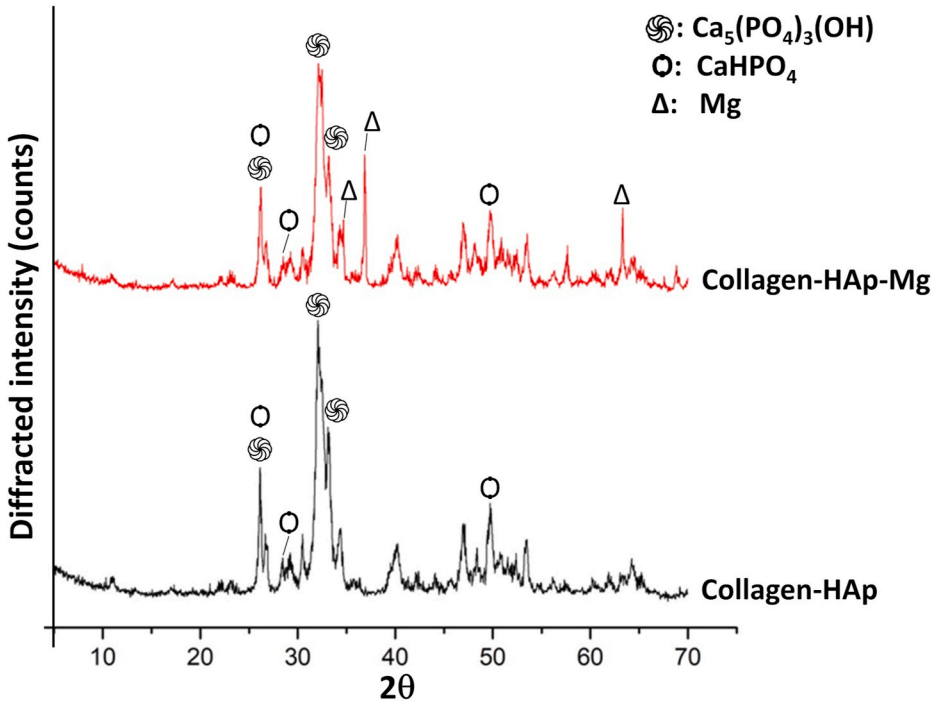

Fig. 4. X-ray diffraction spectra for the composite collagen-HAp and collagen-HAp-Mg biomaterials.

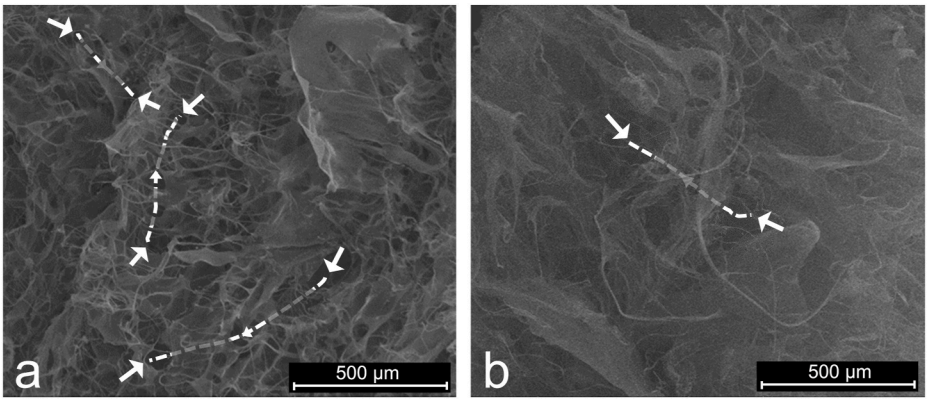

Fig. 5. SEM images of the collagen: (a) surface view, (b) cross-section view. The interconnected pore structure is highlighted by white errors.

within the collagen fibrils in such a way that their c-axes were oriented along the long axes of fibrils, and that the formed hierarchical structure was similar to the one present in the natural bone tissue. The use of Au as third component included in the collagen-HAp composite was also performed in [18]. Mondal et al. [18] reported rapid microwave-assisted synthesis of Au nanoparticles loaded in HAp matrix and successive collagen coating. The drug release properties and cytotoxicity assays were investigated, the latter depending on the Au content. The maximum drug loading efficiency was obtained for 0.1 wt% Au–HAp–Collagen nanoparticles with no cytotoxic effects.

The inclusion of Sr in collagen-HAp matrix represents one of the most studied biocomposite systems. Huang et al. [19] reported collagen fibrils mineralized with Sr^{2+} substituted nano-HAp. The effect of Sr^{2+} on mineralization process was evaluated. Sr^{2+} ions did not influence the organization of apatite crystals and collagen fibrils, however, their addition caused distortions and changes in the apatite crystal latice. Yipin Qi et al. [20] investigated a nanocomposite of type I collagen and Sr-HAp fabricated via a non-canonical biomineralization process. Using polyacrylic acid as a mineralizing director, authors [20] obtained mineralized collagen fibrils, where Sr-HAp occupied interstitial sites. The structural and morphological investigation showed similarities with the hierarchical structure of the natural bone tissue. An *in-vivo* study of Sr/HAp/collagen compound was reported by Kitayama et al. [21]. The aim of authors [21] was to investigate the regeneration effect of a membrane composed of Sr enriched biphasic calcium phosphate (HAp and β-tricalcium phosphate (β-TCP)) and collagen, compared to a non-crosslinked collagen membrane. The bone defects in rabbits treated with the Sr/HAp/collagen membrane showed a significant amount of mineralized new bone compared to the ones treated with the non-cross-linked collagen membrane.

Another third component of collagen-HAp composite reported in literature is zinc (Zn) [22]. Popa et al. [22] concluded based on the results of *in vitro* studies that the obtained Zn doped HAp embedded in collagen matrix had good biocompatibility no cytotoxic effect was observed for HeLa human cancer cells. Weilin Yu et al. [23] developed a novel biomimetic scaffold obtained via lyophilisation process in the form of mesoporous microspheres of Zn-doped HAp dispersed in a collagen matrix. The scaffold was characterized by an interconnected pore structure and a sustained Zn^{2+} ions release, it enhanced the osteogenic differentiation of rat bone marrow-derived mesenchymal stem

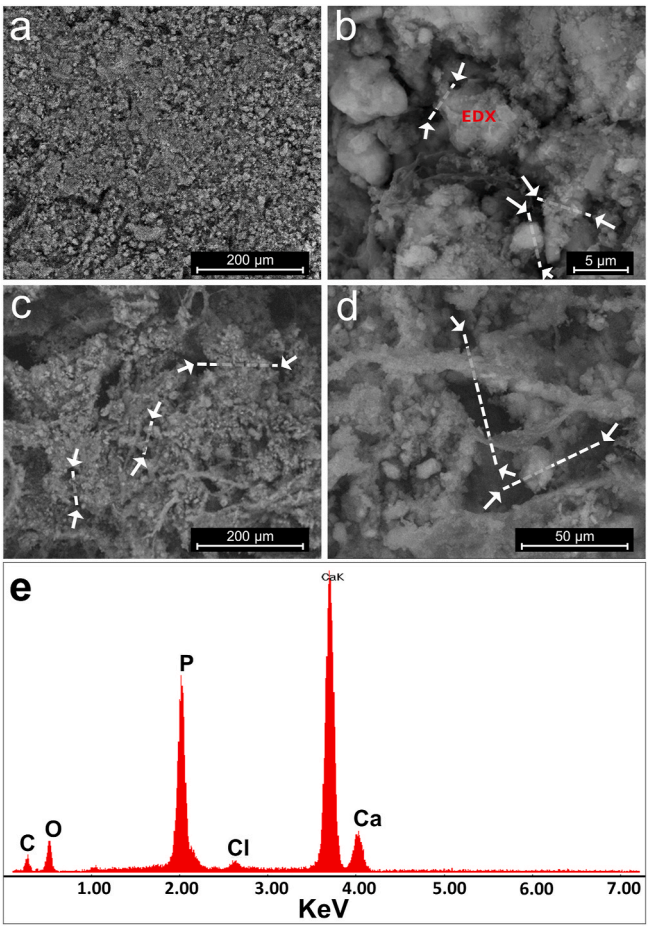

Fig. 6. SEM images of collagen-HAp sample: (a,b) plain view, (c,d) cross-section view, (e) EDX spectrum obtained from the zone evidenced in (b). The interconnected pore structure is highlighted by white errors.

cells. The scaffold also enhanced bone regeneration in femoral condyle defect of a rat model. Song et al. [24] prepared scaffold composed of Zn silicate/nano-HAp/collagen and demonstrated that it significantly enhanced *in vivo* bone regeneration and angiogenesis by activating a pathway in monocytes, compared to HAp/collagen scaffold.

Heinemann et al. [25,26] investigated the effect of silica (SiO_2) addition to obtain a HAp/collagen/SiO_2 composites. A HAp/collagen/SiO_2 xerogel was reported in [25] with a significant improvement of compressive strength (up to 200 MPa) and strain to fracture (up to 11%) due to collagen contribution. In [26], the morphological features of SiO_2/HAp/collagen scaffold, such as surface nanotexture and open porosity, provided optimal conditions for bone marrow stromal cells migration, proliferation and differentiation.

Mg is present in various human organs and has a role in numerous body enzymes. About 60% of Mg is found in bone tissues, constituting about 1% of the total bone mineral content [27] and being attributed as a macro-element. Mg^{2+} ions partially substitute Ca^{2+} ions in biological apatite crystals, and their deficiency can directly affect the bone by altering the structure and size of bone crystals. Mg is of particular importance for bone mass density. Animal and human studies report that Mg deficiency leads to the decrease of bone's mechanical resistance, and, in particularly, promotes micro-fractures, osteoporosis, and fragility [28–32]. Aydın et al. [33] suggest that the lack of Mg might decrease the bone density in postmenopausal women and lead to osteoporosis. Furthermore, the Mg deficiency is connected to the reduced concentration of parathyroid hormone, which plays a role in bone homeostasis. Moreover, Mg lack is associated with the increase of inflammatory proteins (cytokines) negatively effecting bone remodelling. Therefore, the addition of Mg to the bone tissue scaffolds is of particular importance not only to support the bone health, but also for other body health issues [34].

Sartori et al. [35] reported a scaffold realized with type I collagen and Mg-substituted HAp and stabilized with a cross-linking agent bis-epoxyde (1 wt%). The obtained results showed that the scaffold was able to sustain human mesenchymal stem cells (hMSCs) attachment, and to support the formation of new bone and chondral tissue. Roffi et al. [36] investigated a hybrid Mg-doped HAp, collagen, chitosan-based scaffold. In a sheep model, there was no evidence of cartilage and subchondral bone regeneration. In a rabbit model, this scaffold provided less ability to induce tissue healing compared to a commercial one.

In this work, composite of collagen-HAp with the addition of Mg was developed for possible application as orthopaedic material for bone regeneration. Starting from HAp nanopowder, Mg powder, type I collagen (1.00% w/w) and crosslinking agent (glutaraldehyde-AG - 0.25% w/w), two types of composite biomaterials - collagen-HAp and collagen-HAp-Mg were prepared using lyophilisation method. The composites were characterized by Fourier Transform Infrared Spectroscopy (FTIR), X-Ray Diffraction (XRD), Scanning Electron Microscopy (SEM) coupled with Energy Dispersive X-Ray Spectroscopy (EDX) for elemental analysis, and Transmission Electron Microscopy (TEM) coupled with EDX. Time-dependence of *in vitro* biodegradation of composites in SBF solution was investigated.

2. Materials and methods

The developed composite biomaterials had constant concentrations of collagen and crosslinker (glutaraldehyde-AG - 0.25% w/w), and variable concentration of HAp and Mg powders. Before processing, the type I fibrillary collagen gel with the collagen nominal concentration of 2.11% w/w (Sigma-Aldrich) was diluted until 1.00% w/w, and the crosslinking agent (glutaraldehyde-AG - 0.25% w/w) was added. The HAp powder (>95% purity) was purchased from the Plasma Biotal Limited (Tideswell, UK), and the Mg powder (99% purity, granulation of ~500 μm) - from the Strem Chemicals Inc. (Newburyport MA, USA) (shown in Fig. 1). The average particle size of HAp was about 30–60 nm and the particle shape was spherical, while that of Mg was about 200–600 μm and the shape was irregular. The coding and chemical composition of the composite experimental samples was: P1 – 10% collagen and 90% HAp powder; P2 – 10% collagen, 80% HAp and 10% Mg powder.

A flowchart with the processing steps is presented in Fig. 2. The HAp and Mg powders mixture was obtained using Mixer Inversina Bioengineering from Bioengineering AG (Wald, Switzerland) mechanical mixing equipment. By blending the type I collagen gel with the reinforcement additions under the action of a magnetic stirrer with heating, the final composite biomaterials in the form of gels were obtained. The collagen gels were poured into the Petri dishes, placed on the lyophilisation racks and pre-cooled to −40 °C for 90 min. The lyophilisation, an advantageous conditioning technique, which consists in drying the frozen samples by vacuum sublimation of ice, took place for 48 h. The lyophilisation process was carried out by freezing the samples in successive stages, and ice sublimation in advanced vacuum. First, the suspension was frozen at −40 °C for 8 h. Upon drying, the temperature was increased from −40 °C to 10 °C during the first 8 h, and then to 20 °C for the next 10 h and finally up to 30 °C for the subsequent 10 h. The samples were maintained at 30 °C and a pressure of 0.10 mbar for another 4 h until water was removed. In the final drying process, the samples were gently heated to a temperature of 35 °C and a pressure of 0.001 mbar until dried [37–44]. The aspect of the obtained samples is presented in Fig. 2 (right side, (A) collagen-HAp, (B) collagen-HAp-Mg). The size of the cylinders is the following: diameter - 1.5 cm and height −1.8 cm.

FTIR analysis was performed by a JASCO 6200 FT-IR Spectrometer, equipped with a Golden Gate-type attenuated total reflection device

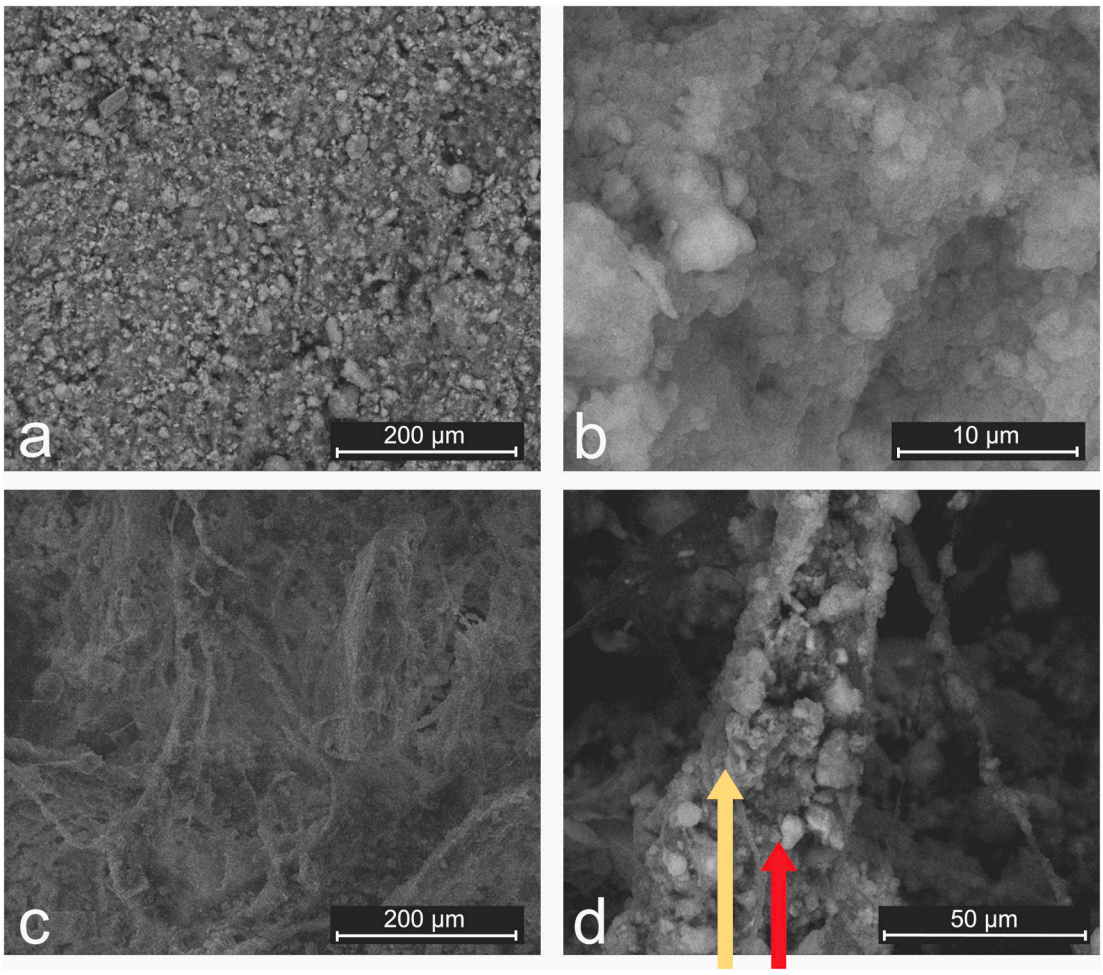

Fig. 7. SEM images of collagen-HAp-Mg sample: (a,b) plain view, (c,d) cross-section view. In (d), the arrows evidence the initial powders particles adhered to the collagen fibrils.

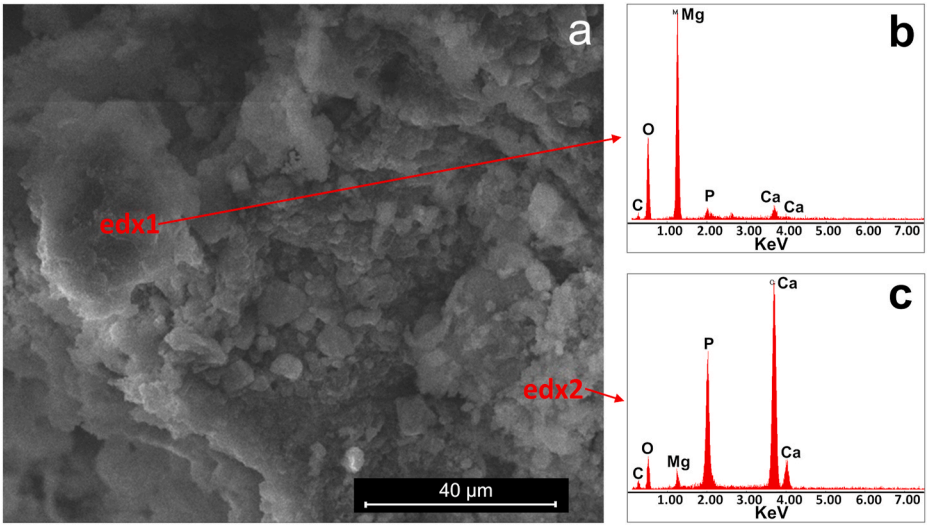

Fig. 8. SEM image of collagen-HAp-Mg sample's plain view (a) and EDX spectra (b,c) obtained from zones evidenced in the image.

(ATR) (Tokyo, Japan). XRD measurements were carried out using a Panalytical X-Pert PRO Diffractometer (Malvern, UK). SEM investigations were performed by QUANTA INSPECT F Scanning Electron Microscope (FEI Company, Eindhoven, Netherlands) working at an acceleration voltage of up to 30 kV and equipped with Energy Dispersive X-Ray Spectrometer Detector (EDAX) with a 132 eV resolution at MnKα. TEM measurements were conducted using a Tecnai F30 high-resolution analytical Transmission Electron Microscope (FEI Company, Eindhoven, Netherlands). The Tecnai F30 was supplied with EDAX XEDS system.

The determination of degradation rate of the composite biomaterials

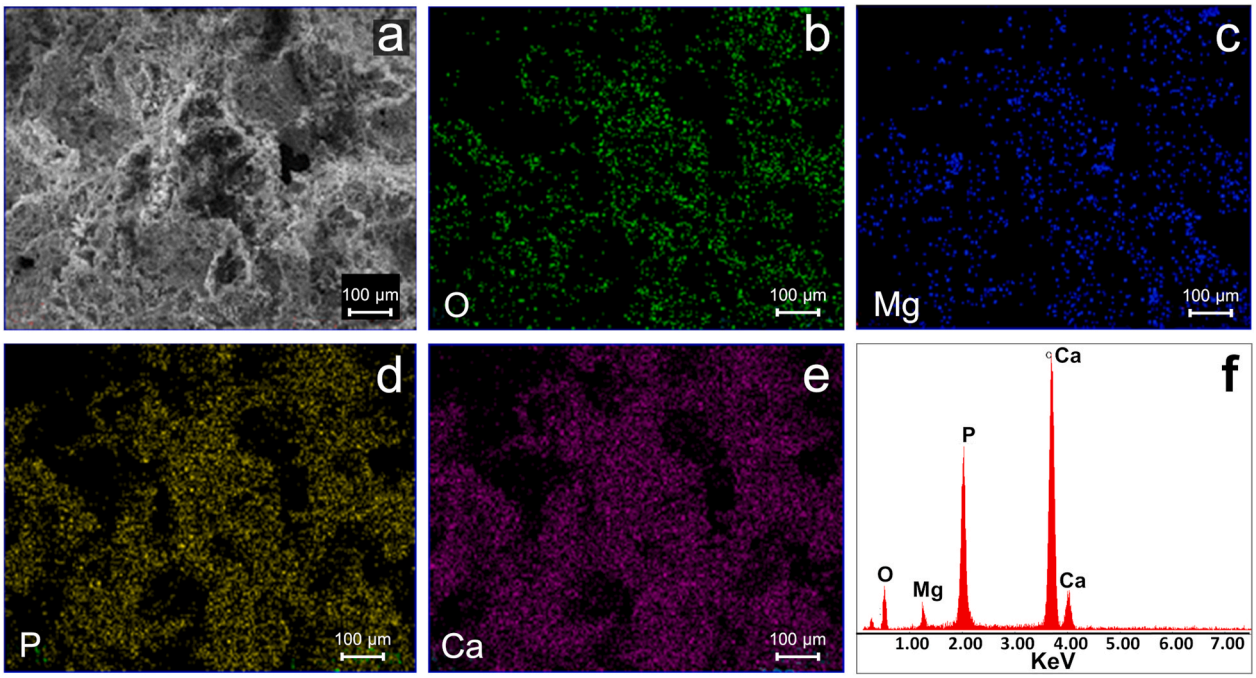

Fig. 9. SEM-EDX mapping of elemental distribution on the collagen-HAp-Mg sample surface (a), O(b), Mg(c), P(d), Ca(e), average spectrum (f) of the zone presented in (a).

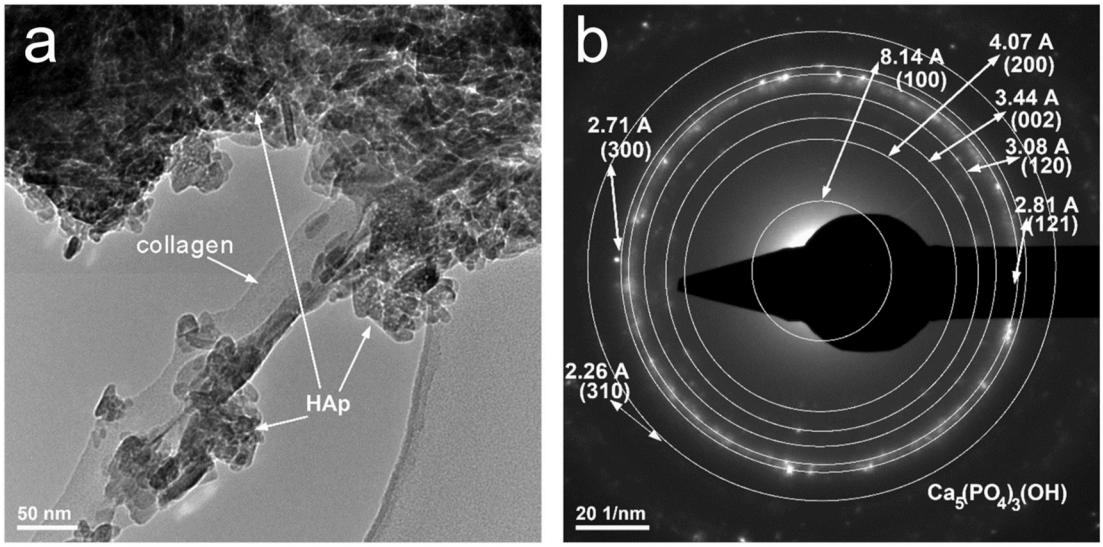

Fig. 10. TEM image in the light field: (a) collagen-HAp sample overview, (b) electron diffraction associated with HAp nanoparticles from (a).

was assessed by measuring the weight loss. Two types of collagen based composite biomaterials (P1 and P2) (Table 1) were tested for biodegradation in the SBF solution (prepared in the laboratory, according to a protocol originally proposed by Kokubo [45,46]) with the pH of 7.4. For measuring weight loss, the cylindrical experimental samples with 0.7 cm height and 1.5 cm diameter were immersed in the SBF for 1, 7, 14, 21 and 28 days. Three experimental runs from each sample were performed for each immersion time. Each sample was immersed in 50 ml of the SBF solution.

The prepared samples were kept in the standard atmosphere for 2 h before the initial weight measurement - M_i (initial mass). After that, they were immersed in the SBF. At each time interval, the samples were removed from the SBF and cleaned with deionized water, stored in the standard atmosphere until the constant weight was reached and weighed (M_t, mass after immersion at time t). The degradation rate (%) was calculated according to the formula shown in Equation (1).

$$R.D. = \frac{M_i - M_t}{M_i} \cdot 100\% \quad (1)$$

where: *R.D.* is the rate of degradation (%), M_i is the initial mass and M_t is the mass after immersion at time t [47–49].

3. Results and discussion

Materials for applications in bone tissue engineering and regenerative medicine should serve as three-dimensional templates and should supply a suitable microenvironment for cell adhesion, proliferation, and differentiation, and new tissue growth. In this investigation, composites

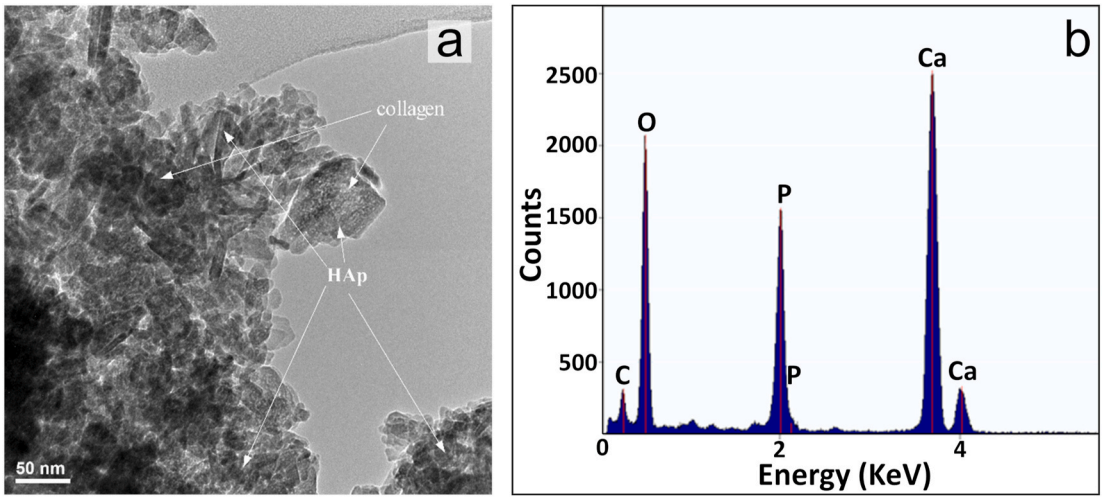

Fig. 11. (a) TEM image in light field: overview aspect on another zone with HAp nanoparticles from collagen-HAp sample, (b) EDX spectrum associated to HAp nanoparticles in (a).

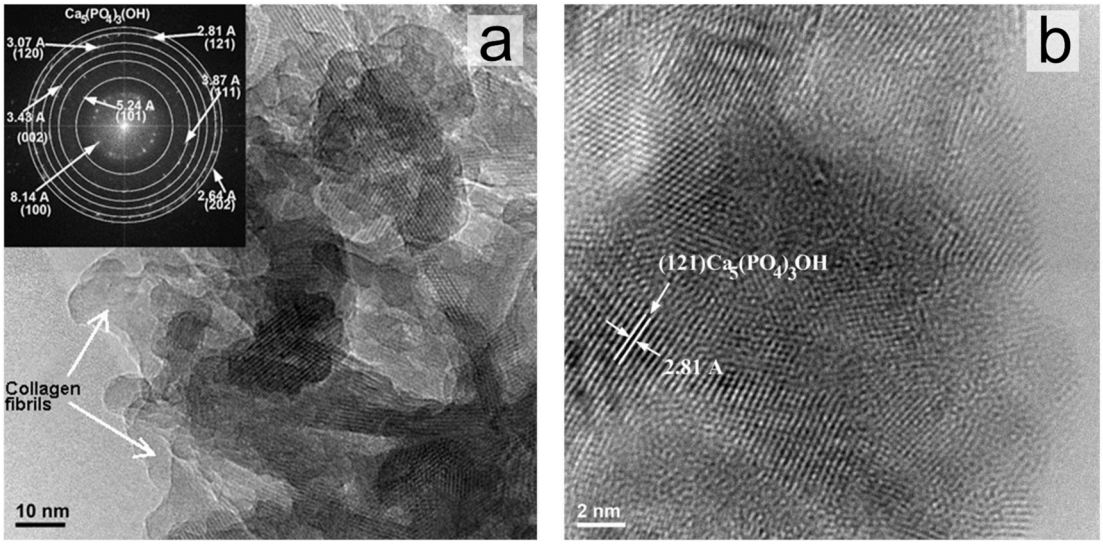

Fig. 12. (a) High resolution TEM image of collagen-HAp sample obtained on a HAp cluster adherent to collagen fibrils, (b) high resolution TEM image of collagen-HAp sample with (121) crystalline plane of HAp.

made from collagen, HAp and Mg were developed, mimicking composition of the bone tissue, and their physico-chemical characteristics were investigated.

3.1. FTIR and XRD analyses

The identification of functional groups in the composite biomaterials was performed by the FTIR spectroscopy. The FTIR spectra are shown in Fig. 3. The spectrum of the collagen alone showed bands for amide I at 1631.48 cm^{-1}, amide II at 1547.59 cm^{-1}, amide III at 1237.11 cm^{-1}, amide A at 3302.5 cm^{-1}, amide B at 3075.9 cm^{-1}, the pyrrolidine rings at 1450.21 cm^{-1} and for the carboxyl group at 1336.43 cm^{-1}. The FTIR spectra for the prepared composite biomaterials revealed bands at ~630 cm^{-1}, ~960 cm^{-1}, ~1090 cm^{-1}, ~1024 cm^{-1}, characteristic for HAp, assigned to the vibrations of the hydroxyl groups OH^{-} and phosphate groups PO_4^{3-}. Bands for amide I (~1649 cm^{-1}), amide II (between 1500 and 1590 cm^{-1}) and pyrrolidine rings (~1450 cm^{-1}) from the collagen structure were also registered [50–53].

X-ray powder diffraction patterns, characteristic for the prepared composite biomaterials (P1 and P2) are presented in Fig. 4. P1 sample is characterized by the presence of the main phase - $Ca_5(PO_4)_3(OH)$, HAp, with attributed peaks at $2\Theta = 25.7°$ (002), $2\Theta = 31.85°$ (211), and $2\Theta = 32.98°$ (300) (PCPDF number 73–1731); and minor phase - $CaHPO_4$, monocalcium phosphate, with attributed peaks at $2\Theta = 26.52°$ (200), $2\Theta = 28.5°$ (-1-1 2) and $2\Theta = 49.1°$ (−3 2 1) (PCPDF number 77–0128).

P2 sample (collagen-HAp-Mg), in addition to the HAp and $CaHPO_4$ phases, is characterised by the presence of the Mg phase, with the attributed peaks at $2\Theta = 32.2$ (100), $2\Theta = 36.78$ (101) and $2\Theta = 63.06$ (103) (PCPDF number 85–0821).

3.2. Morphological analyses

3.2.1. SEM analysis

The morphology of the samples obtained after the lyophilisation process was investigated by SEM. In Fig. 5, the morphology of the control collagen sample is presented. From the plain (a) and cross-section (b) view, the interconnected pore structure is well visible.

The P1 sample's plain and cross-section views are presented in Fig. 6. Also in this case, the pores of 20–40 μm can be well observed ((d)). The collagen fibrils and adherent HAp particles can be well distinguished on

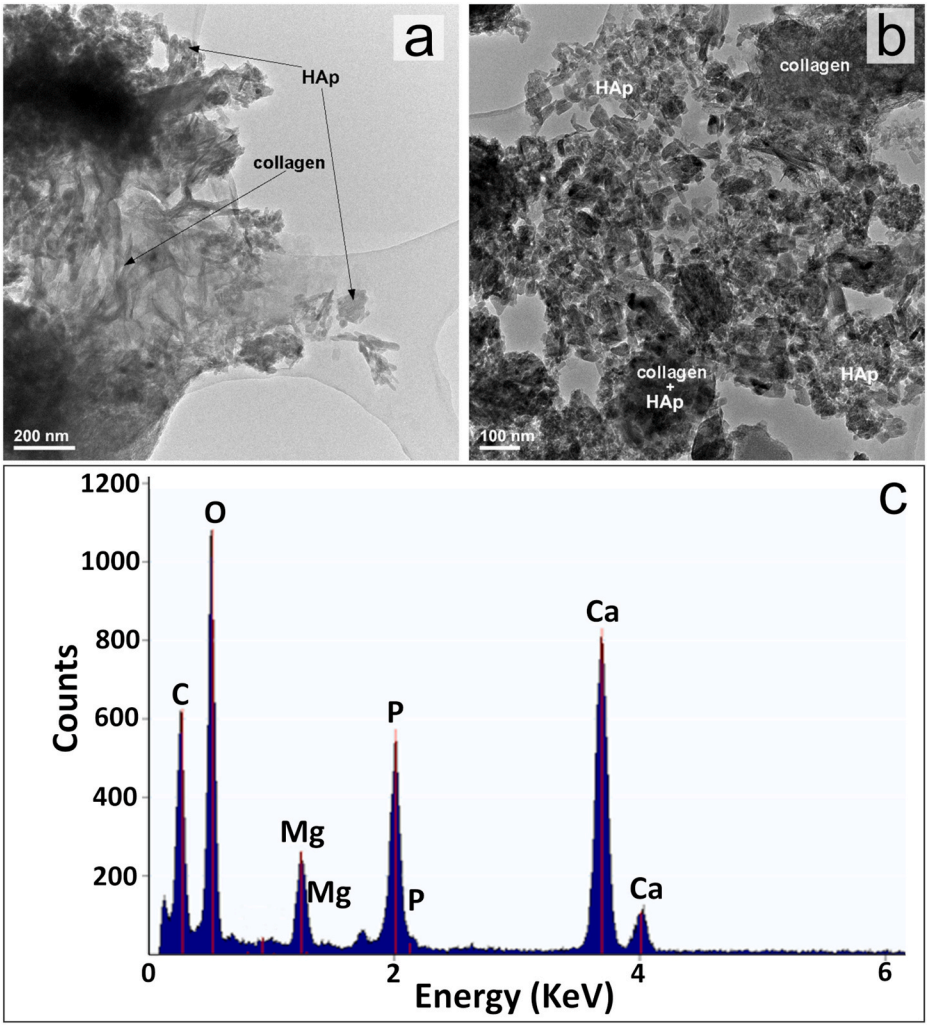

Fig. 13. (a and b) TEM images in light field of collagen-HAp-Mg sample at different magnifications, (c) EDX spectrum obtained on area with HAp and Mg nanoparticles.

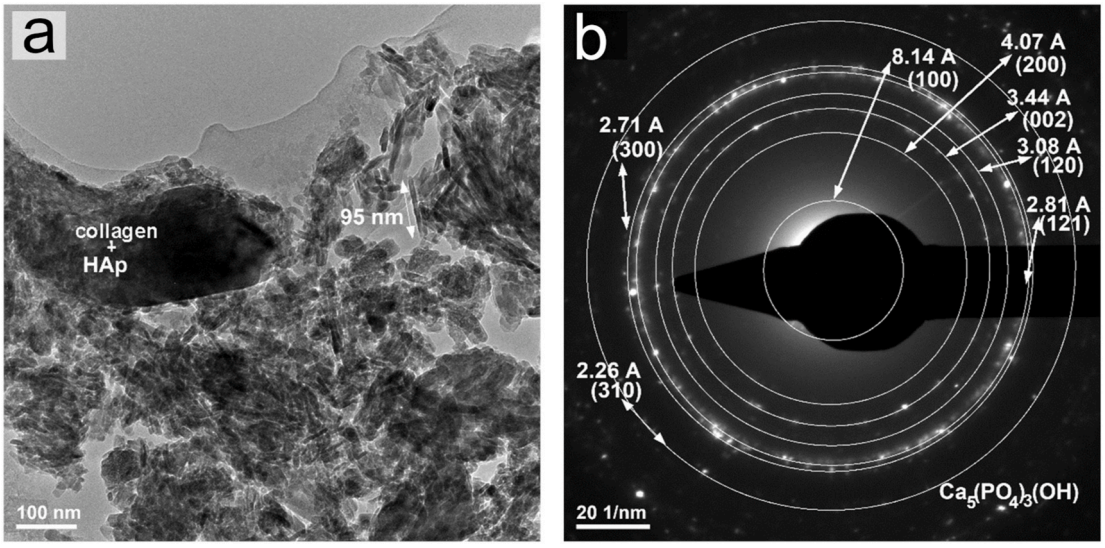

Fig. 14. (a) TEM images in light field of collagen-HAp-Mg sample; (b) the electron diffraction associated with area with HAp nanoparticles from (a).

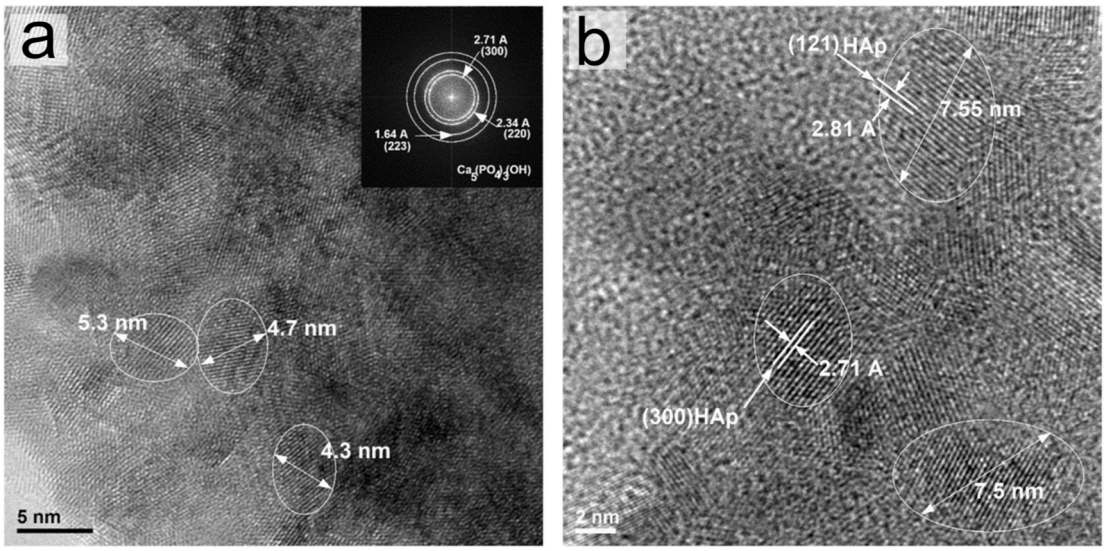

Fig. 15. (a and b) High resolution TEM images obtained on areas with HAp nanoparticles corresponding to collagen-HAp-Mg sample.

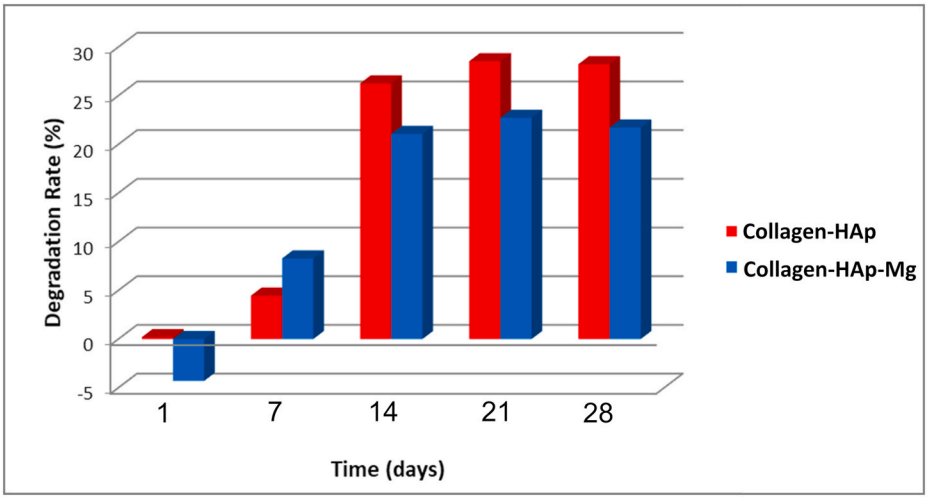

Fig. 16. Evolution of degradation rate of collagen-HAp and collagen-HAp-Mg at 1, 7, 14, 21, 28 days of immersion in SBF.

the cross-section image of the P1 sample ((c-d)). The EDX spectrum obtained from the zone evidenced in the image accounts for the presence of elements constituents of HAp.

In Fig. 7, SEM images of plain and cross-section views of the P2 composite are presented. In the cross-section images (c) and, particularly, in (d), the collagen fibrils and the particles of HAp and Mg attached to them can be observed. To support this observation, EDX spectra of several P2 sample zones were registered and presented in Fig. 8, accounting on the presence of HAp and Mg particles.

As can be observed from Fig. s 6–8, the prepared P1 and P2 samples are characterized by a homogeneous aspect with HAp particles homogeneously distributed and adherent to the collagen matrix. To check for the homogeneity of the Mg distribution, the SEM-EDX mapping of elemental distribution on the P2 sample surface is presented in Fig. 9. As follows from (c), Mg particles are homogeneously distributed within the P2 composite.

The microstructural characteristics of the prepared P1 and P2 composites reported here, and namely their chemical composition, including collagen, HAp phase, a minor admixture of $CaHPO_4$, and Mg, and their interconnected pore structure with homogeneous distribution of HAp and Mg particles, adhered to the collagen fibrils, are important for bone tissue engineering applications. Indeed, bone consists of a matrix of type I collagen and calcium phosphate mineral (CdHAp) as reinforcing phase. One of the substitutions for Ca^{2+} ions in the HAp lattice are Mg^{2+} ions [54]. In this investigation, Mg powder was added to the composite, instead of Mg^{2+} ions substitution in the hydroxyapatite as done by authors [55], reporting that Mg^{2+} ions were introduced to obtain a specific substitution percentage of calcium. In the case of Sr^{2+} substitution [19], this did not influence the organization of apatite crystals and collagen fibrils. However, the distortions in the apatite crystal structure were registered.

According to authors [54], in an adult human bone, HAp crystal dimensions range between 10 and 40 nm, depending on the reflection used. In this work, TEM analysis was applied to determine HAp nanoparticles characteristic dimensions in the prepared composites.

3.2.2. *TEM analysis*

Nanostructural aspects of the P1 and P2 samples were confirmed by TEM coupled with EDX. In Fig. 10, a nanostructural aspect of an area of the P1, where collagen fibrils and adherent HAp cluster nanoparticles are present, is shown. The electron diffraction corresponding to an area with HAp nanoparticles in (a) is shown in (b), confirming that the particles are nanocrystalline. The electron diffraction indexing demonstrates that nanocrystallites belong to the HAp phase with hexagonal

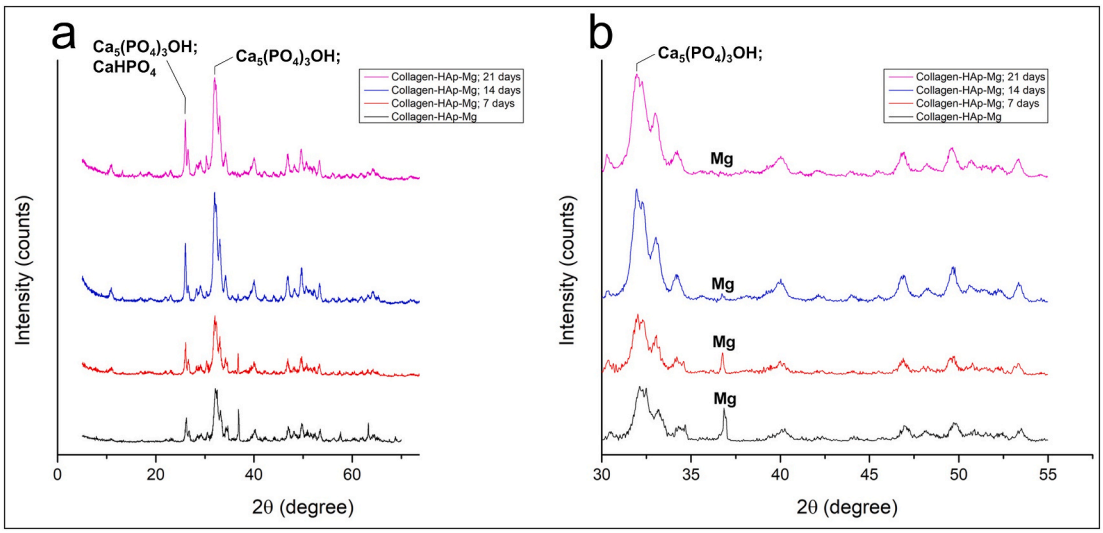

Fig. 17. (a) XRD patterns of collagen-HAp-Mg sample immersed in SBF for 7, 14 and 21 days; (b) XRD patterns with the angular range adjacent to the main Mg peak at 2θ = 36.78°, corresponding to collagen-HAp-Mg sample maintained in SBF for 7, 14 and 21 days.

Table 2
The main results of the study.

	FTIR analysis	XRD analysis	SEM-EDX analysis	TEM-EDX analysis	pH	Degradation after 28 days
Collagen-HAp before immersion in SBF	bands attributable to HAp and collagen (amide I, amide II)	HAp – main phase, $CaHPO_4$ - admixture.	Homogeneously distributed HAp particles adherent to collagen fibrils. Interconnected pore structure.	HAp nanocrystallites associated in clusters (4–5 nm) adherent to collagen fibrils.	7.1	-
Collagen-HAp after immersion in SBF	-	HAp – main phase, $CaHPO_4$ - admixture.	-	-	7.1	28%
Collagen-HAp-Mg before immersion in SBF	bands attributable to HAp and collagen (amide I, amide II)	HAp – main phase, $CaHPO_4$ – admixture Mg phase.	Homogeneously distributed HAp and Mg particles adherent to collagen fibrils. Interconnected pore structure.	HAp nanocrystallites associated in clusters (4–5 nm) and Mg nanoparticles adherent to collagen fibrils.	8.2	–
Collagen-HAp-Mg after immersion in SBF	-	HAp – main phase, $CaHPO_4$ – admixture.	-	-	9.5	21%

crystalline lattice, according to the ICDD PDF number 09–0080.

In Fig. 11(a), another area with HAp nanoparticles associated with a structural characteristic of the P1 sample is highlighted: HAp cluster nanoparticles adhering to the collagen fibrils. The local elemental EDX analysis (Fig. 11(b)) showed the presence of the Ca, P and O elements, constituents of HAp. The carbon (C) originates from both the collagen fibrils and the amorphous carbon film deposited on the sample holder.

The nanocrystalline nature of the HAp particles is also highlighted by the high resolution TEM images, shown in Fig. 12. In (a), areas with parallel fringes, associated to the families of crystalline planes belonging to the HAp nanocrystallites (clusters of 4–5 nm of diameter) are highlighted. The insert in Fig. 12(a), corresponding to the Fourier Transform processing, attests that the interplanar distances correspond to HAp. A clearer emphasis on the nanocrystalline nature of the HAp particles in the P1 is shown in Fig. 12(b), where the Miller indices (121) crystalline plane family of the HAp is highlighted.

To summarize, the P1 sample is nanostructured, composed of HAp nanocrystallites associated in clusters of 4–5 nm of diameter adhering to the collagen fibrils.

Aspects of the P2 sample nanostructure are present in the TEM images demonstrated in Fig. 13(a and b). The existence of nanoparticles of acicular or platelet shape present in clusters adhering to the collagen fibrils is detected. The EDX spectrum presented in Fig. 13(c) accounts for the presence of Ca, P and O (from HAp) and Mg elements.

The aspect of the composite P2 nanostructure is shown in Fig. 14(a), in which the length of a HAp acicular shaped particle (95 nm) is estimated. The electron diffraction (Fig. 14(b)) associated with HAp particles in (a) highlights the nanocrystalline character of the sample. The indexing of the electron diffraction image shows that nanocrystals belong to the HAp hexagonal crystalline lattice according to the ICDD chart number 04-016-1647.

The high resolution TEM images in Fig. 15(a and b) confirm the nanocrystalline nature of the HAp particles. The nanocrystalites with the dimensions of 4–8 nm are highlighted. The Fourier Transform processing results shown in the insert of Fig. 15(a) demonstrate the presence of groups of parallel fringes (associated with the crystalline planes) with interplanar distances corresponding to the HAp compound with hexagonal crystalline lattice. Two nanocrystals with different families of crystalline planes of the Miller indices (300) and (121) of the HAp are also revealed in Fig. 15(b).

To summarize, the P2 composite contains a nanocrystalline HAp phase, consisting of agglomerated nanocrystallites of 4–8 nm adhering to the collagen fibrils. The local elemental chemical analysis carried out by EDX confirmed the presence of the Mg nanoparticles in the sample.

In order to regenerate bone, bone tissue engineering requires the use of materials with functional properties, and nano-HAp holds great promise for biological effects [56], for example, nanoparticles can optimise interactions with bone proteins and proper nanoparticle shape can achieve a special control on cell behaviour. Moreover, the resorption rate of composite materials can be modified by changes in crystallinity and composition of nano-HAp, fitting in this way the bone formation rate. Also, it is important to highlight that the high specific surface area of nanomaterials leads to a higher reactivity in adsorbing proteins, growth factor, etc [57].

3.3. Degradation study

Determination of the degradation rate of the developed composite materials was performed by measuring the weight loss. The evolution of the degradation rate of P1 and P2 registered at 1, 7, 14, 21, 28 days of immersion in SBF is presented in Fig. 16. It can be noticed that, in the case of P1, the degradation process began within the first 24 h of immersion, whereas, in the case of sample P2, absorption took place during the first 24 h, while the effective degradation started in the following days reaching a value of about 8% on the 7th day of immersion. During the following period, the P2 composite exhibited a lower rate of degradation, which is desirable in terms of *in vivo* conditions because bone substitution material has to degrade slowly during the healing process. As can be seen from Fig. 16, at day 14 the degradation rate of both composites reached a plateau.

The pH variation in the solutions of P1 and P2 had a different behaviour (see Table 1). In the case of the P1, the pH stabilized after 24 h around 7.08, whereas, in the case of the P2 sample, it increased at day 28 up to 9.47. The pH increase in the P2 solution was due to the presence of the Mg ions, which formed $Mg(OH)_2$ in aqueous solutions. In the presence of Cl^- ions from the SBF, $Mg(OH)_2$ converted into $MgCl_2$, soluble in the medium and, thus, a process of alkalinisation of the medium took place. The XRD spectra of P2 sample at 7, 14 and 21 days of degradation highlight the occurring transformations, accompanied by the Mg peak intensity decrease (Fig. 17).

The XRD patterns obtained from P2 immersed in the SBF for 7, 14 and 21 days are present in Fig. 17(a). The main Mg (101) peak at $2\theta = 36.78^\circ$, corresponding to the interplanar distance of 2.44 Å, had a decreasing relative intensity trend depending on the immersion time in the SBF, and disappearing completely at day 21.

The evolution of the Mg main peak for the immersed samples is more clearly visible in Fig. 17(b), in which the angular range adjacent to the main Mg peak is present.

Therefore, the role of the Mg addition in this investigation consists in not only the beneficial effects on bone and whole body, but also in 25% decrease in the degradation rate for the collagen-HAp-Mg composite compared to the collagen-HAp one, effects otherwise attained by crosslinking agents [55].

The results obtained in this study are briefly summerized in Table 2.

4. Conclusions

Collagen and biological apatites are assembled in mineralized collagen fibrils in the natural bone and teeth tissues. In this work, the composite scaffolds of collagen(10%)-HAp(90%) and collagen(10%)-HAp(80%)-Mg(10%) were prepared by lyophilisation method and characterized. The prepared composites were characterized by a homogeneous aspect with HAp nanocrystallites (4–8 nm) and their clusters homogeneously distributed and adherent to the collagen matrix. In the collagen(10%)-HAp(80%)-Mg(10%) composite, the distribution of the Mg nanoparticles was homogeneous.

The *in vitro* degradation in the SBF solution attested the release of Mg from collagen(10%)-HAp(80%)-Mg(10%) composite during the period of up to 21 days. This composite exhibits 25% lower degradation rate with respect to the composite without Mg, which is desirable for *in vivo* conditions because bone material has to degrade slowly during the healing process and the new bone formation.

The developed composite materials, composed of collagen with interconnected pore structure and nano-HAp and Mg particles adherent to the type 1 collagen fibrils, are promising for applications as bone substitutes favouring bone healing and regeneration. Future investigations will include *in vitro* cell tests and *in vivo* animal studies.

CRediT authorship contribution statement

Iulian V. Antoniac: Conceptualization, Data curation, Funding acquisition, Resources, Supervision, Validation, Writing – review & editing. **Aurora Antoniac:** Data curation, Methodology, Investigation, Validation, Writing – review & editing. **Eugeniu Vasile:** Investigation, Writing – original draft. **Camelia Tecu:** Investigation. **Marco Fosca:** Investigation, Writing – original draft. **Viktoriya G. Yankova:** Supervision, Validation. **Julietta V. Rau:** Conceptualization, Supervision, Validation, Writing – original draft, Writing – review & editing.

Declaration of competing interest

The authors declare no conflict of interest.

Acknowledgements

This work was funded by a grant of the Romanian Ministry of Research and Innovation, CCCDI-UEFISCDI, Project COFUND-M-ERA. NET II-BiogenInk/70/2017, within PNCDI III.

The technical assistance of Mr. Luca Imperatori, Mr. Marco Ortenzi, and Mr. Massimo Di Menno Di Bucchianico is gratefully acknowledged.

References

[1] R.F. Canadas, S. Pina, A.P. Marques, J.M. Oliveira, R.L. Reis, Cartilage and bone regeneration—how close are we to bedside? Transl. Regen. Med. Clin. (2016) 89–106.

[2] Y.-Z. Huang, H.-Q. Xie, X. Li, Scaffolds in Bone Tissue Engineering: Research Progress and Current Applications, Encyclopedia of Bone Biology, 2020, pp. 204–215.

[3] M.A. Velasco, C.A. Narváez-Tovar, D.A. Garzón-Alvarado, Design, materials, and mechanobiology of biodegradable scaffolds for bone tissue engineering, BioMed Res. Int. (2015) 1–21, https://doi.org/10.1155/2015/729076.

[4] G. Turnbull, J. Clarke, F. Picard, P. Riches, L. Jia, F. Han, B. Li, W. Shu, 3D bioactive composite scaffolds for bone tissue engineering, Bioact. Mater. 3 (2018) 278–314, https://doi.org/10.1016/j.bioactmat.2017.10.001.

[5] Ö. Kalenderer, A. Turgut, Bone, Musculoskeletal Research and Basic Science, 2016, pp. 303–321.

[6] J.V. Rau, A. Generosi, S. Laureti, V.S. Komlev, D. Ferro, S.N. Cesaro, B. Paci, V. R. Albertini, E. Agostinelli, S.M. Barinov, Physicochemical investigation of pulsed laser deposited carbonated hydroxyapatite films on titanium, ACS Appl. Mater. Interfaces 1 (2009) 1813–1820, https://doi.org/10.1021/am900356e.

[7] M.D. O'Donnell, Y. Fredholm, A. de Rouffignac, R.G. Hill, Structural analysis of a series of strontium-substituted apatites, Acta Biomater. 4 (2008) 1455–1464, https://doi.org/10.1016/j.actbio.2008.04.018.

[8] C. Capuccini, P. Torricelli, F. Sima, E. Boanini, C. Ristoscu, B. Bracci, G. Socol, M. Fini, I.N. Mihailescu, A. Bigi, Strontium-substituted hydroxyapatite coatings synthesized by pulsed-laser deposition: in vitro osteoblast and osteoclast response, Acta Biomater. 4 (2008) 1885–1893, https://doi.org/10.1016/j.actbio.2008.05.005.

[9] F. Ren, Y. Leng, R. Xin, X. Ge, Synthesis, characterization and ab initio simulation of magnesium-substituted hydroxyapatite, Acta Biomater. 6 (2010) 2787–2796, https://doi.org/10.1016/j.actbio.2009.12.044.

[10] A. Tampieri, G.C. Celotti, E. Landi, M. Sandri, Magnesium doped hydroxyapatite: synthesis and characterization, Key Eng. Mater. 264–268 (2004) 2051–2054. https://doi.org/10.4028/www.scientific.net/KEM.264-268.2051.

[11] E. Landi, G. Logroscino, L. Proietti, A. Tampieri, M. Sandri, S. Sprio, Biomimetic Mg-substituted hydroxyapatite: from synthesis to in vivo behaviour, J. Mater. Sci. Mater. Med. 19 (2007) 239–247, https://doi.org/10.1007/s10856-006-0032-y.

[12] E. Boanini, P. Torricelli, M. Fini, A. Bigi, Osteopenic bone cell response to strontium-substituted hydroxyapatite, J. Mater. Sci. Mater. Med. 22 (2011) 2079–2088, https://doi.org/10.1007/s10856-011-4379-3.

[13] G. Spence, N. Patel, R. Brooks, N. Rushton, Carbonate substituted hydroxyapatite: resorption by osteoclasts modifies the osteoblastic response, J. Biomed. Mater. Res. 90A (2009) 217–224, https://doi.org/10.1002/jbm.a.32083.

[14] J. Wang, C. Liu, Biomimetic collagen/hydroxyapatite composite scaffolds: fabrication and characterizations, J. Bionic Eng. 11 (2014) 600–609, https://doi.org/10.1016/s1672-6529(14)60071-8.

[15] R. Socrates, N. Sakthivel, A. Rajaram, U. Ramamoorthy, S.N. Kalkura, Novel fibrillar collagen–hydroxyapatite matrices loaded with silver nanoparticles for orthopedic application, Mater. Lett. 161 (2015) 759–762, https://doi.org/10.1016/j.matlet.2015.09.089.

[16] D. Predoi, S.L. Iconaru, M. Albu, C.C. Petre, G. Jiga, Physicochemical and antimicrobial properties of silver-doped hydroxyapatite collagen biocomposite, Polym. Eng. Sci. 57 (2017) 537–545, https://doi.org/10.1002/pen.24553.

[17] S. Aryal, K.C. Remant Bahadur, S.R. Bhattarai, P. Prabu, H.Y. Kim, Immobilization of collagen on gold nanoparticles: preparation, characterization, and hydroxyapatite growth, J. Mater. Chem. 16 (2006) 4642–4648, https://doi.org/10.1039/b608300e.

[18] S. Mondal, G. Hoang, P. Manivasagan, M.S. Moorthy, T.T. Vy Phan, H.H. Kim, T. P. Nguyen, J. Oh, Rapid microwave-assisted synthesis of gold loaded hydroxyapatite collagen nano-bio materials for drug delivery and tissue engineering application, Ceram. Int. 45 (2019) 2977–2988, https://doi.org/10.1016/j.ceramint.2018.10.016.

[19] Z. Huang, F. Cui, Q. Feng, X. Guo, Incorporation of strontium into hydroxyapatite via biomineralization of collagen fibrils, Ceram. Int. 41 (2015) 8773–8778, https://doi.org/10.1016/j.ceramint.2015.03.102.

[20] Y. Qi, S. Mai, Z. Ye, C. Aparicio, Biomimetic fabrication and characterization of collagen/strontium hydroxyapatite nanocomposite, Mater. Lett. 274 (2020) 127982, https://doi.org/10.1016/j.matlet.2020.127982.

[21] S. Kitayama, L.O. Wong, L. Ma, J. Hao, S. Kasugai, N.P. Lang, N. Mattheos, Regeneration of rabbit calvarial defects using biphasic calcium phosphate and a strontium hydroxyapatite-containing collagen membrane, Clin. Oral Implants Res. 27 (2016) e206–e214, https://doi.org/10.1111/clr.12605.

[22] C.L. Popa, C.M. Bartha, M. Albu, R. Guégan, M. Motelica-Heino, et al., Synthesis, characterization and cytotoxicity evaluation on zinc doped hydroxyapatite in collagen matrix, Dig. J. Nanomater. Biostruct. 10 (2015) 681–691, insu-01363294.

[23] W. Yu, T.-W. Sun, C. Qi, Z. Ding, H. Zhao, S. Zhao, Z. Shi, Y.-J. Zhu, D. Chen, Y. He, Evaluation of zinc-doped mesoporous hydroxyapatite microspheres for the construction of a novel biomimetic scaffold optimized for bone augmentation, Int. J. Nanomed. 12 (2017) 2293–2306, https://doi.org/10.2147/ijn.S126505.

[24] Y. Song, H. Wu, Y. Gao, J. Li, K. Lin, B. Liu, X. Lei, P. Cheng, S. Zhang, Y. Wang, J. Sun, L. Bi, G. Pei, Zinc silicate/nano-hydroxyapatite/collagen scaffolds promote angiogenesis and bone regeneration via the p38 MAPK pathway in activated monocytes, ACS Appl. Mater. Interfaces 12 (2020) 16058–16075, https://doi.org/10.1021/acsami.0c00470.

[25] S. Heinemann, T. Coradin, H. Worch, H.P. Wiesmann, T. Hanke, Possibilities and limitations of preparing silica/collagen/hydroxyapatite composite xerogels as load-bearing biomaterials, Compos. Sci. Technol. 71 (2011) 1873–1880, https://doi.org/10.1016/j.compscitech.2011.08.023.

[26] S. Heinemann, C. Heinemann, M. Jäger, J. Neunzehn, H.P. Wiesmann, T. Hanke, Effect of silica and hydroxyapatite mineralization on the mechanical properties and the biocompatibility of nanocomposite collagen scaffolds, ACS Appl. Mater. Interfaces 3 (2011) 4323–4331, https://doi.org/10.1021/am200993q.

[27] G. Della Pepa, Microelements for bone boost: the last but not the least, Clin. Cases Miner. Bone Metab. (2016) 181–185, https://doi.org/10.11138/ccmbm/2016.13.3.181.

[28] R.K. Rude, F.R. Singer, H.E. Gruber, Skeletal and hormonal effects of magnesium deficiency, J. Am. Coll. Nutr. 28 (2009) 131–141, https://doi.org/10.1080/07315724.2009.10719764.

[29] Y. Toba, Y. Kajita, R. Masuyama, Y. Takada, K. Suzuki, S. Aoe, Dietary magnesium supplementation affects bone metabolism and dynamic strength of bone in ovariectomized rats, J. Nutr. 130 (2000) 216–220, https://doi.org/10.1093/jn/130.2.216.

[30] K.L. Tucker, M.T. Hannan, H. Chen, L.A. Cupples, P.W.F. Wilson, D.P. Kiel, Potassium, magnesium, and fruit and vegetable intakes are associated with greater bone mineral density in elderly men and women, Am. J. Clin. Nutr. 69 (1999) 727–736, https://doi.org/10.1093/ajcn/69.4.727.

[31] M.-H. Kim, J.-Y. Yeon, M.-K. Choi, Y.J. Bae, Evaluation of magnesium intake and its relation with bone quality in healthy young Korean women, Biol. Trace Elem. Res. 144 (2011) 109–117, https://doi.org/10.1007/s12011-011-9044-7.

[32] S. Castiglioni, A. Cazzaniga, W. Albisetti, J. Maier, Magnesium and osteoporosis: current state of knowledge and future research directions, Nutrients 5 (2013) 3022–3033, https://doi.org/10.3390/nu5083022.

[33] H. Aydın, O. Deyneli, D. Yavuz, H. Gözü, N. Mutlu, I. Kaygusuz, S. Akalın, Short-term oral magnesium supplementation suppresses bone turnover in postmenopausal osteoporotic women, Biol. Trace Elem. Res. 133 (2009) 136–143, https://doi.org/10.1007/s12011-009-8416-8.

[34] J. Vormann, Magnesium: nutrition and metabolism, Mol. Aspect. Med. 24 (2003) 27–37, https://doi.org/10.1016/s0098-2997(02)00089-4.

[35] M. Sartori, S. Pagani, A. Ferrari, V. Costa, V. Carina, E. Figallo, M.C. Maltarello, L. Martini, M. Fini, G. Giavaresi, A new bi-layered scaffold for osteochondral tissue regeneration: in vitro and in vivo preclinical investigations, Mater. Sci. Eng. C 70 (2017) 101–111, https://doi.org/10.1016/j.msec.2016.08.027.

[36] A. Roffi, E. Kon, F. Perdisa, M. Fini, A. Di Martino, A. Parrilli, F. Salamanna, M. Sandri, M. Sartori, S. Sprio, A. Tampieri, M. Marcacci, G. Filardo, A composite chitosan-reinforced scaffold fails to provide osteochondral regeneration, Int. J. Mol. Sci. 20 (2019), https://doi.org/10.3390/ijms20092227.

[37] M. Geiger, Collagen sponges for bone regeneration with rhBMP-2, Adv. Drug Deliv. Rev. 55 (2003) 1613–1629, https://doi.org/10.1016/j.addr.2003.08.010.

[38] S.D. Figueiro, J.C. Goes, R.A. Moreira, A.S.B. Sombra, On the physico-chemical and dielectric properties of glutaraldehyde crosslinked galactomannan-collagen films, Carbohydr. Polym. 56 (2004) 313–320, https://doi.org/10.1016/j.carbpol.2004.01.011.

[39] Water and aqueous solutions at subzero temperature, in: H.D. Lüdemann, F. Franks (Eds.), aus: Water - A Comprehensive Treatise, vol. 7, Plenum Press, New York and London, 1982, https://doi.org/10.1002/bbpc.19830870724, 484 Seiten, Berichte der Bunsengesellschaft für physikalische Chemie 87 (1983) 621-621.

[40] I.V. Antoniac, M.G. Albu, A. Antoniac, L.C. Rusu, M.V. Ghica, Collagen–bioceramic smart composites, in: I.V. Antoniac (Ed.), Handbook of Bioceramics and Biocomposites, Springer International Publishing AG Switzerland, 2016, pp. 301–324.

[41] T.V. Burjanadze, Thermodynamic substantiation of water-bridged collagen structure, Biopolymers 32 (1992) 941–949, https://doi.org/10.1002/bip.360320805.

[42] J. Bella, B. Brodsky, H.M. Berman, Hydration structure of a collagen peptide, Structure 3 (1995) 893–906, https://doi.org/10.1016/s0969-2126(01)00224-6.

[43] P. Szpak, Fish bone chemistry and ultrastructure: implications for taphonomy and stable isotope analysis, J. Archaeol. Sci. 38 (2011) 3358–3372, https://doi.org/10.1016/j.jas.2011.07.022.

[44] M.G. Albu, Collagen Gels and Matrices for Biomedical Applications, LAP LAMBERT Academic 23-24 Publishing GmbH & Co. KG, Saarbrücken, Germany, 2011, ISBN 978-3-8443-3057-1.

[45] T. Kokubo, H. Takadama, How useful is SBF in predicting in vivo bone bioactivity? Biomaterials 27 (2006) 2907–2915, https://doi.org/10.1016/j.biomaterials.2006.01.017.

[46] ISO/FDIS 23317, Implants for surgery - in vitro evaluation for apatite-forming ability of implant materials. https://www.iso.org/standard/41446.html, 2007.

[47] A. Sionkowska, J. Kozłowska, Characterization of collagen/hydroxyapatite composite sponges as a potential bone substitute, Int. J. Biol. Macromol. 47 (2010) 483–487, https://doi.org/10.1016/j.ijbiomac.2010.07.002.

[48] F. Wenpo, L. Gaofeng, F. Shuying, Q. Yuanming, T. Keyong, Preparation and characterization of collagen–hydroxyapatite/pectin composite, Int. J. Biol. Macromol. 74 (2015) 218–223, https://doi.org/10.1016/j.ijbiomac.2014.11.031.

[49] K.R. Mohamed, A.A. Mostafa, Preparation and bioactivity evaluation of hydroxyapatite-titania/chitosan-gelatin polymeric biocomposites, Mater. Sci. Eng. C 28 (2008) 1087–1099, https://doi.org/10.1016/j.msec.2007.04.040.

[50] L.F. Sukhodub, C. Moseke, L.B. Sukhodub, B. Sulkio-Cleff, V.Y. Maleev, M. A. Semenov, E.G. Bereznyak, T.V. Bolbukh, Collagen–hydroxyapatite–water interactions investigated by XRD, piezogravimetry, infrared and Raman spectroscopy, J. Mol. Struct. 704 (2004) 53–58, https://doi.org/10.1016/j.molstruc.2003.12.061.

[51] M.C. Chang, J. Tanaka, FT-IR study for hydroxyapatite/collagen nanocomposite cross-linked by glutaraldehyde, Biomaterials 23 (2002) 4811–4818, https://doi.org/10.1016/s0142-9612(02)00232-6.

[52] A. Dong, P. Huang, W.S. Caughey, Protein secondary structures in water from second-derivative amide I infrared spectra, Biochemistry 29 (2002) 3303–3308, https://doi.org/10.1021/bi00465a022.

[53] M. Kikuchi, S. Itoh, S. Ichinose, K. Shinomiya, J. Tanaka, Self-organization mechanism in a bone-like hydroxyapatite/collagen nanocomposite synthesized in vitro and its biological reaction in vivo, Biomaterials 22 (2001) 1705–1711, https://doi.org/10.1016/s0142-9612(00)00305-7.

[54] S.R. Stock, The mineral–collagen interface in bone, Calcif. Tissue Int. 97 (2015) 262–280, https://doi.org/10.1007/s00223-015-9984-6.

[55] A. Nicoletti, M. Fiorini, J. Paolillo, L. Dolcini, M. Sandri, D. Pressato, Effects of different crosslinking conditions on the chemical–physical properties of a novel bio-inspired composite scaffold stabilised with 1,4-butanediol diglycidyl ether (BDDGE), J. Mater. Sci. Mater. Med. 24 (2012) 17–35, https://doi.org/10.1007/s10856-012-4782-4.

[56] B. Lowe, J.G. Hardy, L.J. Walsh, Optimizing nanohydroxyapatite nanocomposites for bone tissue engineering, ACS Omega 5 (2019) 1–9, https://doi.org/10.1021/acsomega.9b02917.

[57] S. Padilla, I. Izquierdo-Barba, M. Vallet-Regí, High specific surface area in nanometric carbonated hydroxyapatite, Chem. Mater. 20 (2008) 5942–5944, https://doi.org/10.1021/cm801626k.